Electronic Supplementary Information

High-capacity polymeric electrodes for potassium batteries

Vahid Ramezankhani,[a] Igor K. Yakuschenko,[b] Sergey Vasilyev,[b] Tatiana A. Savinykh,[b] Alexander V. Mumyatov,[b] Ivan S. Zhidkov,[c,d] Elena V. Shchurik,[b] Ernst Z. Kurmaev,[c,d] Alexander F. Shestakov,[b] and Pavel A. Troshin[e,b]*

[a] Skolkovo Institute of Science and Technology, Bolshoy Bulvar 30, Moscow, 143026, Russian Federation

[b] Institute for Problems of Chemical Physics, Russian Academy of Sciences (IPCP RAS). Chernogolovka, Moscow Region, 142432, Russian Federation. Email: troshin@icp.ac.ru

[c] Institute of Physics and Technology, Ural Federal University, Mira 9 str., 620002 Yekaterinburg, Russia.

[d] M. N. Mikheev Institute of Metal Physics of Ural Branch of Russian Academy of Sciences, S. Kovalevskoi 18 str., 620108 Yekaterinburg, Russia.

[e] Silesian University of Technology, Akademicka 2A, 44-100 Gliwice, Poland

1. Experimental Section

1.1 Materials and instrumentation

Chemicals and solvents were purchased from Sigma-Aldrich and used as received. Chemical analysis was performed on a CHNS/O elemental analyzer «Vario Micro cube» Elementar GmbH. FTIR spectra were recorded with PerkinElmer Spectrum BX 100 instrument. The solid-state NMR experiments were performed on a Bruker AVANCE III spectrometer operating at 400 and 101 MHz for ^{1}H and ^{13}C, respectively, using a 3.2 mm MAS probe at room temperature. The chemical shifts are specified relative to TMS at 0 ppm. Conventional cross-polarization (CP) experiments were used for the acquisition of the ^{13}C NMR spectra with the spinning rate of 14-16 kHz under ^{1}H SPINAL-64 decoupling. The duration of ^{1}H π/2 pulse was 2.5 μs, contact time 1000 μs. The surface properties of the materials were analysed using Quadrasorb SI instrument (USA). XPS core-level measurements were performed using a PHI 5000 Versa Probe XPS spectrometer (ULVAC Physical Electronics, USA) based on a classic X-ray optic scheme with a hemispherical quartz monochromator and an energy analyzer working in the range of binding energies from 0 to 1500 eV. The apparatus uses electrostatic focusing and magnetic screening to achieve an energy resolution of $\Delta E \leq 0.5$ eV.

1.2 Synthesis of polymers

*1.2.1 Synthesis of polymer **P1***

3,3'-Diaminobenzidine (1.29, 6 mmol) was added to a suspension of 1.98 g (6 mmol) of triquinoyl hydrate in 100 ml of glacial AcOH stirred at 60 °C. The mixture was further stirred for 1 h at 60 °C and then another 5 h at 100–105 °C. After cooling, a brown precipitate was filtered off, washed on a filter successively with 30 ml of ice-cold AcOH, 30 ml of 10% aqueous AcOH, 50 ml of water and 30 ml of methanol. The remaining powder was dried at room temperature in vacuum over P_2O_5. The crude product (2.00 g) was further stirred with 50 ml of DMF at 80–85 °C for 4 hours, filtered and successively washed on the filter with 150 ml (5 x 30 ml) of hot DMF, 150 ml (5 x 30 ml) of methanol and 150 ml (5 x 30 ml) of acetone. After drying at room temperature in a vacuum over phosphorous anhydride, the compound **P1** (1.89 g)

was annealed in a vacuum at 180 °C for 4 h to remove the hydrated water. The target compound **P1** was obtained with a yield of 1.67 g (~90% of the theoretical yield). FTIR spectrum (v, cm^{-1}): 3392, 1710, 1616, 1492, 1361, 1195, 1086, 1061, 890, 832, 789. Elemental analysis: calculated for $C_{18}H_{12}N_4O_5$, %: C 59.34, H 3.32, N 15.38, O 21.96; found, %: C 60.43, H 3.72, N 15.80.

*1.2.2 Synthesis of polymer **P2***

1,2,4,5-Tetraaminobenzene tetrahydrochloride (0.92 g, 3.24 mmol) was added to a suspension of 1.07 g (3.24 mmol) of triquinoyl hydrate in 50 ml of glacial AcOH stirred at 50 °C. The mixture was stirred at the same temperature for 1 h, then 1.06 g (12.93 mmol) of anhydrous sodium acetate was added and the reaction mixture was stirred at 100–105 °C for another 5 h. After cooling, 50 ml of water was added to the reaction mixture and the formed precipitate was isolated by filtration. The crude material was washed on the filter with water until the filtrate becomes colorless and dried in a vacuum over P_2O_5. The dried crude product (0.85 g) was stirred with 35 ml of DMF at 80–85 °C for 4 h. After cooling, the precipitate was collected by filtration and washed on a filter successively with 150 ml (5 x 30 ml) of DMF, 150 ml (5 x 30 ml) of methanol, 150 ml (5 x 30 ml) of acetone and dried in a vacuum at room temperature over phosphorous anhydride. The resulting powder (0.66 g) was annealed in a vacuum at 150 °C for 5 h. The target compound **P2** was obtained with a yield of 0.55 g (73% of the theoretical). FTIR spectrum (v, cm^{-1}): 3204, 1621, 1469, 1354, 1252, 1051, 881, 752. Elemental analysis: calculated for $C_{12}H_6N_4O_4$, %: C 53.34; H 2.24; N, 20.74; O 23.69; found, %: C 52.83; H 2.44; N 22.53.

*1.2.3 Synthesis of polymer **P3***

2,6-Diaminoantraquinone (1.43 g, 6.0 mmol) and triquinoyl hydrate (0.99 g, 3.0 mmol) were successively added to a mixture of N-methylpyrrolidone (30 ml) and glacial AcOH (30 ml) stirred at 45-50 °C. The mixture was stirred at the same temperature for 1 h and then at 100-110 °C for another 5 h. After cooling, the reaction mixture was diluted with an equal volume of water (60 ml), the precipitate was filtered off, washed with water until the filtrate becomes colorless (150 ml) followed by acetone (20 ml) and dried in air. The crude product (1.49 g) was suspended in 30 ml of dimethylformamide, stirred 1 h at 55-60 °C and the precipitate was isolated by filtration; this procedure was repeated three times. Afterward, the crude

product was treated three times with acetone in the same way at 45-50 °C. After drying in vacuum over phosphorous anhydride, the target product **P3** was obtained with a yield of 0.82 g (24% of the theoretical). FTIR spectrum (v, cm^{-1}): 3427, 3321, 3202, 1659, 1623, 1565, 1359, 1322, 1284, 1153, 890, 840, 740, 660, 546 (Fig. S1f). Elemental analysis: calculated for $C_{34}H_{14}N_4O_7$, %: C 67.10; H 2.63; N, 9.21, found, %: C 68.50; H 4.29; N, 11.06.

*1.2.4 Synthesis of polymer **P4***

p-Phenylenediamine (0.86 g, 8 mmol) was added in one portion to the suspension of 2.50 g (8 mmol) of triquinoyl hydrate in 150 ml of glacial acid stirred at 60 °C. The resulting mixture was stirred at 60-65 °C for 2 h and then another 5 h at 100-110 °C. After cooling, 150 ml of water was added, the mixture was stirred for 2 h at room temperature and the resulting precipitate was isolated by filtration. The filtrate was washed on the filter with water until the filtrate became colorless, followed by methanol (50 ml) and acetone (50 ml). Polymer **P4** was obtained in the form of a hydrate (three water molecules per polymer unit) with a yield of 1.10 g (56% of the theoretical value). FTIR spectrum (v, cm^{-1}): 3442, 2978, 2636, 1579, 1459, 1409, 1172, 1059, 1026. Elemental analysis, found, %: C 50.51; H 3.90; N 9.78.

*1.2.4 Synthesis of polymer **P5***

p-Phenylenediamine 1.30 g (12 mmol) was added in one portion to a suspension of 1.98 g (6 mmol) of triquinoyl hydrate in 100 ml of glacial AcOH stirred at 50-60 °C. The mixture was stirred at the same temperature for 1 h and then at 100 °C for another 5 h. After cooling, the reaction mixture was diluted with an equal volume of water and the formed precipitate was isolated by filtration. The crude product was washed on the filter with water until the filtrate became colorless, dried in air to a constant weight (1.81 g). Then, the material was stirred with 60 ml of DMF at 50-60 °C for 5 h, the solids were filtered off and successively washed on the filter with 150 ml (5 x 30 ml) of DMF, 150 ml (5 x 30 ml) of methanol, 150 ml (5 x 30 ml) of acetone. The residue was dried in a vacuum over phosphorous anhydride at room temperature and then additionally at 150–160 °C in a vacuum oven for 5 h. The target product **P5** was obtained with a yield of 1.09 g (60% of the theoretical value). FTIR spectrum (v, cm^{-1}): 3317, 1675, 1603, 1513, 1407, 1314, 1252, 1175, 1019, 827. Elemental analysis, found, %: C 56.68; H 4.20; N 13.68.

1.2.5 Synthesis of polymer **P6**

p-Phenylenediamine 1.08 g (18 mmol) was added in one portion to a suspension of 1.98 g (6 mmol) of triquinoyl hydrate in 120 ml of glacial AcOH stirred at 50 °C. The mixture was stirred at the same temperature for 1 h and then at 100-105 °C for another 5 h. After cooling, the reaction mixture was diluted with an equal volume of water and the formed precipitate was isolated by filtration. The crude product was washed on the filter with water until the filtrate became colorless and dried in air to a constant weight (1.38 g). Then, the material was stirred with 60 ml of DMF at 70-80 °C for 5 h, the solids were filtered off and successively washed on the filter with 150 ml (5 x 30 ml) of DMF, 150 ml (5 x 30 ml) of methanol, and 150 ml (5 x 30 ml) of acetone. The residue was dried in a vacuum over phosphorous anhydride at room temperature and then additionally at 160–170 °C in a vacuum oven for 5 h. The target product **P6** was obtained with a yield of 0.82 g (36% of the theoretical value). FTIR spectrum (v, cm^{-1}): 3052, 1670, 1601, 1512, 1407, 1312, 1244, 1176, 1059, 1023, 974, 829. Elemental analysis, found, %: C 57.75; H 4.11; N 14.22.

1.3 Potassium half-cells

Coin-type cells (CR2032) were used to characterize electrochemical properties of the polymers. The positive electrodes were prepared the following way. The PVDF binder (20 mg, Gelon Lib) was stirred with 1.5 mL of N-methyl-2-pyrrolidone (NMP) for 30 min. Then, well-grinded active material (one of polymers **P1-P6**,100 mg) and conductive filler (80 mg, super-P, Gelon Lib) were added to the PVDF in NMP. The mixture was stirred at room temperature for 12 h and the resulting slurry was cast on Al/C foil (Gelon Lib) by an automatic tape coating machine and dried for 8h inside the vacuum oven. The active mass loading for all polymers was ~0.3 mg/cm^2 (except when stated otherwise). To assemble the batteries, well-dried round-shape (d=16 mm) composite electrodes were transferred into the Ar-filled MBRaun glove box (H_2O and O_2<0.1 ppm). The negative electrodes were prepared by pressing well-washed metallic potassium (150-170 mg) on a steel spacer (2 cm^2). Glass fiber filter (WHATMAN, 1 layer) was used as a separator. Then, 110 µL of the electrolyte represented by the 2.2 M solution of KPF_6 in diglyme was applied on the steel spacer. Half-cells were cycled repeatedly within the voltage window of 0.7-4V.

The fabricated potassium half-cells were characterized by potentiostatic measurements (cyclic voltammetry) using Biologic VMP3 instrument and by galvanostatic measurements (charge-discharge cycling) using the battery analyzer BTS-5V (Neware Technology Ltd.).

Before performing the final measurements, the cells were preconditioned in galvanostatic regime at the current density of 0.5 A g^{-1} until the specific capacity value was stabilized. Initial evolution of the specific capacity was attributed to the SEI formation and electrode activation. Typically, such preconditioning required several tens or even hundreds of cycles (depending on the material activation behaviour).

1.4 ATR-FTIR measurements

A dry and clean piece of potassium (90 mg) was dissolved in 0.25 M solution of naphthalene in diglyme (1 mL) to obtain a dark green solution. Pristine electrodes, containing 90 wt % of the active material and 10 wt. % of carboxymethyl cellulose (CMC) binder were soaked in the resulting solution (1 mL) for 12 h. Afterward, the electrodes were washed 3 times with dimethoxyethane (5 ml each time) and dried in a vacuum antechamber. All the aforementioned procedures were performed in the Ar-filled glove box. The ATR-FTIR measurements were performed for pristine and metallated electrodes using Bruker Compact FTIR Spectrometer ALPHA II equipped with a diamond prism.

1.5 DFT calculations

To gain a deeper insight into the structure and energetics of products formed by metallation of polymers **P1-P6** under electrochemical reduction in potassium half-cells, we performed quantum chemical calculations using the PBE electron density functional [S1] with the SBK pseudopotential [S2] and extended basis C, N, O: [5s, 5p, 2d/3s, 3p, 2d], Li, K: [4s, 1p/2s, 1p], H: [5s, 1p/3s, 1p] for valence electrons [S3]. The Hirschfeld method [S4] was used to calculate the atomic charges. For broadening of peaks in IR spectra Lorentz shape with the fixed linewidth of 10 cm^{-1} was used. All calculations were performed in the Priroda software [S3] and using the facilities of the Joint Supercomputer Center of the Russian Academy of Sciences.

For modeling the polymers **P1-P6**, the model oligomeric structures comprised of 1-2 repeating units were selected and optimized (Figure T1).

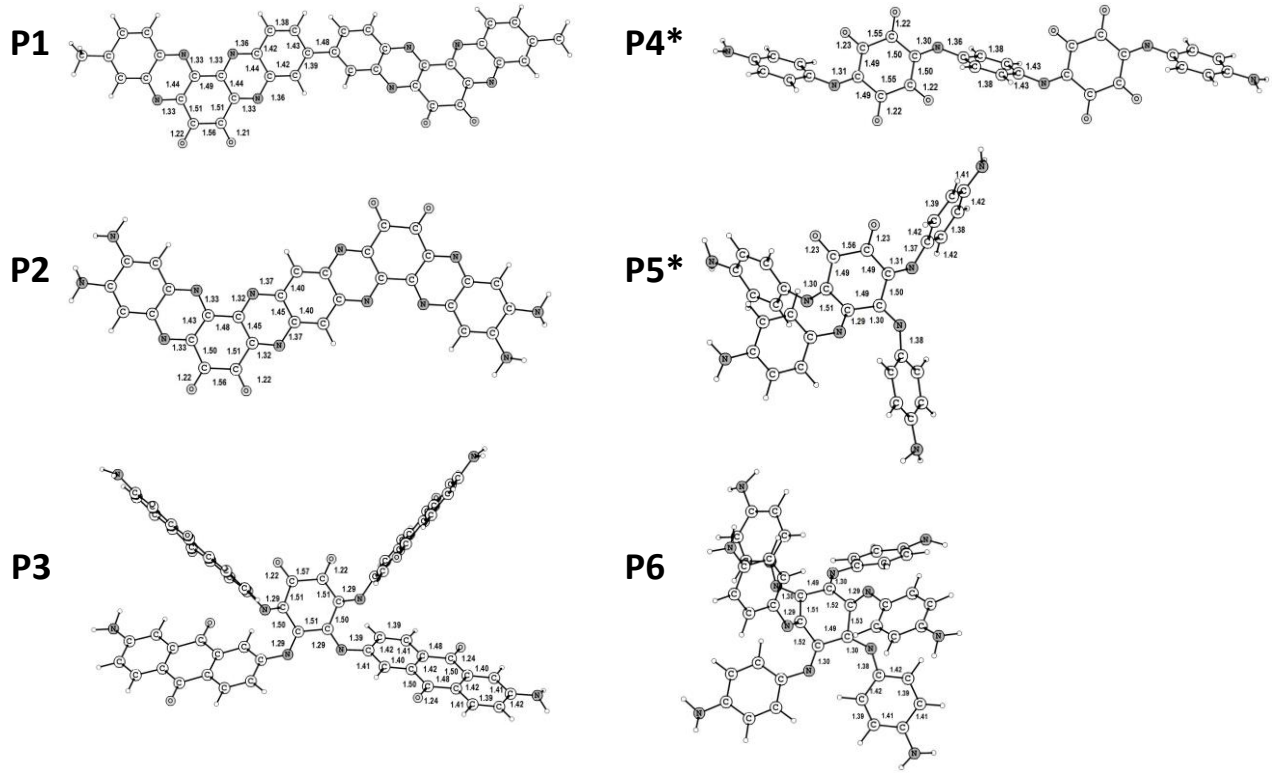

Fig. T1. The optimized molecular frameworks, which model the structures of polymers **P1-P6**. Note that only one among many possible arrangements of the building blocks in **P4-P6** were selected for calculation.

The linear polymers **P1** and **P4*** (**P4*** is one of the possible model structures of **P4**, see discussion in the main text) have non-planar structures due to the steric hindrance effects. In **P1**, the C-C-C-C dihedral angle between the repeating units is 35°. The angle between the adjacent C_6 rings in **P4*** is 56°. Notably, **P1** possesses two rotational isomers differing by the relative orientations of CO groups in two adjacent repeating units: on the same side of the polymer chain or directed in opposite directions. These isomers have almost the same energy.

In all calculated structures, the carbonyl groups leave the plane of the cycle to reduce the coulombic repulsion between the electronegative oxygen atoms. The same applies to the nitrogen atoms of the imino groups. Both O and N atoms bear comparable charges of ca. -0.15.

The calculated FTIR spectra (see Fig. S2) are in good agreement with the experimental ones. In the **P1** spectrum, the band at 1697 cm^{-1} corresponds to in-phase and antiphase vibrations v(C=O). An intense peak at 1630 cm-1 corresponds to (C-C) vibrations of the phenyl ring. Peaks at 1482 and 1446 cm^{-1} correspond mainly to the v (C-N) vibrations in the cycle, whereas the vibration bands ar 1338, 1288, 1214, 1130, and 1040 cm^{-1} are due to various stretching C-C vibrations of the cycle. The 825 cm^{-1} band represents in-plane deformation cycle vibrations, while the 609 cm^{-1} band is assigned to the out-of-plane deformation cycle vibrations.

In the **P2** spectrum, the 1680 cm^{-1} band corresponds to in-phase and antiphase vibrations v(C = O).. The peak at 1503 cm^{-1} corresponds to stretching C-N vibrations and C-C vibrations of the phenyl ring. The peaks at 1286 and 1204 cm^{-1} correspond mainly to v(C-N) vibrations in the cycle, whereas the vibration bands at 1046 and 859 cm^{-1} are due to in-plane deformation C-C vibrations of the cycle. The signatures at 737 and 668 cm^{-1} correspond to the out-of-plane bending vibrations of cycles.

In the **P3** spectrum, the 1674 cm^{-1} band corresponds to in-phase and antiphase vibrations v (C = O) of anthraquinone. The band 1614 cm^{-1} is due to the in-plane bending vibrations of terminal NH_2 and C-C cycle vibrations. The 1516 cm^{-1} band corresponds to in-phase and antiphase (C=N) stretching vibrations. The peaks at 1453, 1318 and 1275 cm^{-1} correspond to stretching C-C vibrations of the cycles. The peaks at 1144, 1013, 976 and 873 cm^{-1} are assigned to in-plane deformation cycle vibrations. The bands at 819, 738 cm^{-1} are due to the out-of-plane deformation cycle oscillations, whereas the peaks at 441 and 417 cm^{-1} correspond to the out-of-plane deformation vibrations of the terminal NH_2-groups.

For the model structure **P4*** with two repeating units, there are intense vibration bands at 1622 and 1429 cm^{-1}, which correspond to v(C = O) vibrations and stretching vibrations of C – N –C groups, respectively. The peak at 1511 cm^{-1} also corresponds to vibrations of C-N –C groups. The peak at 1251 cm^{-1} corresponds to the bending vibrations of the C_6-ring linked to N atoms as well as symmetric stretching vibrations of C-N-C bonds. More intense bands at 1153 and 978 cm^{-1} are due to the vibrations of the two cycles. Weakly pronounced peaks at 809-525 cm^{-1} correspond to the out-of-plane bending vibrations of C-N-C groups and associated cycles.

In the **P5*** spectrum (**P5*** is one of the possible model structures of **P5**, see discussion in the main text), the 1620 cm^{-1} band corresponds to in-phase and out-of-phase v(C=O) vibrations. The bands at 1494 and 1461 cm^{-1} correspond to stretching in-phase and

antiphase (C=N) vibrations. The peaks at 1301 and 1162 cm^{-1} correspond to in-plane vibrations of the phenyl ring, whereas the band at 1005 cm^{-1} is due to the in-plane vibrations of the C_6-cycle and the peak at 809 cm^{-1} is due to out-of-plane bending vibrations of the phenyl ring. The peaks at 587 and 537 cm^{-1} are assigned to the out-of-plane deformation vibrations of the terminal NH_2-groups.

In the **P6*** spectrum (**P6*** is one of the possible model structures of **P6**, see discussion in the main text), the 1625 cm^{-1} band corresponds to the deformation vibrations of the terminal amino groups $\delta(NH_2)$. The 1537 and 1498 cm^{-1} cm^{-1} bands correspond to the stretching vibrations of C=N bonds. The peaks at 1284 and 1158 cm^{-1} correspond to in-plane vibrations of the phenyl ring, whereas the bands at 1081 and 981 cm^{-1} are due to in-plane vibrations of the central C_6-cycle and 807 cm^{-1} is assigned to out-of-plane bending vibrations of the phenyl ring. The peak at 570 cm^{-1} corresponds to the out-of-plane bending vibrations of terminal NH_2 groups.

The calculation of the specific metallation energies of the polymer (P) models, δE_{2n}, was carried out based on the calculated attachment energies of the corresponding number of diatomic K_2 molecules

$$P + n\,K_2 = PK_{2n} + \Delta E_{2n}$$

and the experimental value of sublimation energy of potassium in the form of diatomic molecules, which leads to the following relationship:

$$\delta E_{2n} = \Delta E_{2n}/2n - 15.1 \text{ kcal/mol}$$

To estimate the contribution of the effects of intermolecular interactions, the structures of supramolecular dimers of **P1-P2** and **P4*** with 6 attached K atoms per repeating unit were optimized (Fig. S10, Fig. S11c). The calculated dimerization energies are 4.82, 4.73, and 6.52 eV for **P1**, **P2**, and **P4***, respectively. We can assume that the same total number of pair interactions for each polymer repeating unit is realized in the three-dimensional structure of an organic cathode, which allows us to estimate the specific values of the metallation energy given in parentheses in Table S1.

Table S1. Surface properties of **P1-P6**

Polymer	BET method		Barrett-Joyner-Halenda (BJH) method		t-plot method		
	SSA[1)] $m^2 g^{-1}$	Volume of pores[2)] $cm^3 g^{-1}$	V_{MEP}[3)] $cm^3 g^{-1}$	d (nm)	V_{MIP}[4)] $cm^3 g^{-1}$	S_{MIP} $m^2 g^{-1}$	S_{MEP} $m^2 g^{-1}$
P1	21.3	0.084	0.079	23.6	0.004	9.45	11.8
P2	27.2	0.14	0.14	3.56	0.00	0.00	27.2
P3	4.87	0.013	0.012	3.45	0.00	0.00	4.87
P4	3.79	0.019	0.018	3.49	0.00	1.13	2.66
P5	11.6	0.082	0.082	30.3	0.00	0.25	11.4
P6	6.98	0.017	0.014	4.45	0.00	2.94	4.05

[1] SSA – specific surface area
[2] Calculated at P/P_0=0.99
[3] MIP – micropores
[4] MEP - mesopores

Table S2. The calculated metallation energies δE_{2n} for models of polymes **P1**, **P2**, and **P4*** given in eV per introduced K^+ ion. The energies estimated for supramolecular dimers of the fully metallated structures are given in parathesis.

n	**P1**	**P2**	**P4***
2	1.66	1.58	2.03
4	1.05	0.97	1.17
6	0.73 (1.53)	0.67 (1.46)	0.87 (1.95)

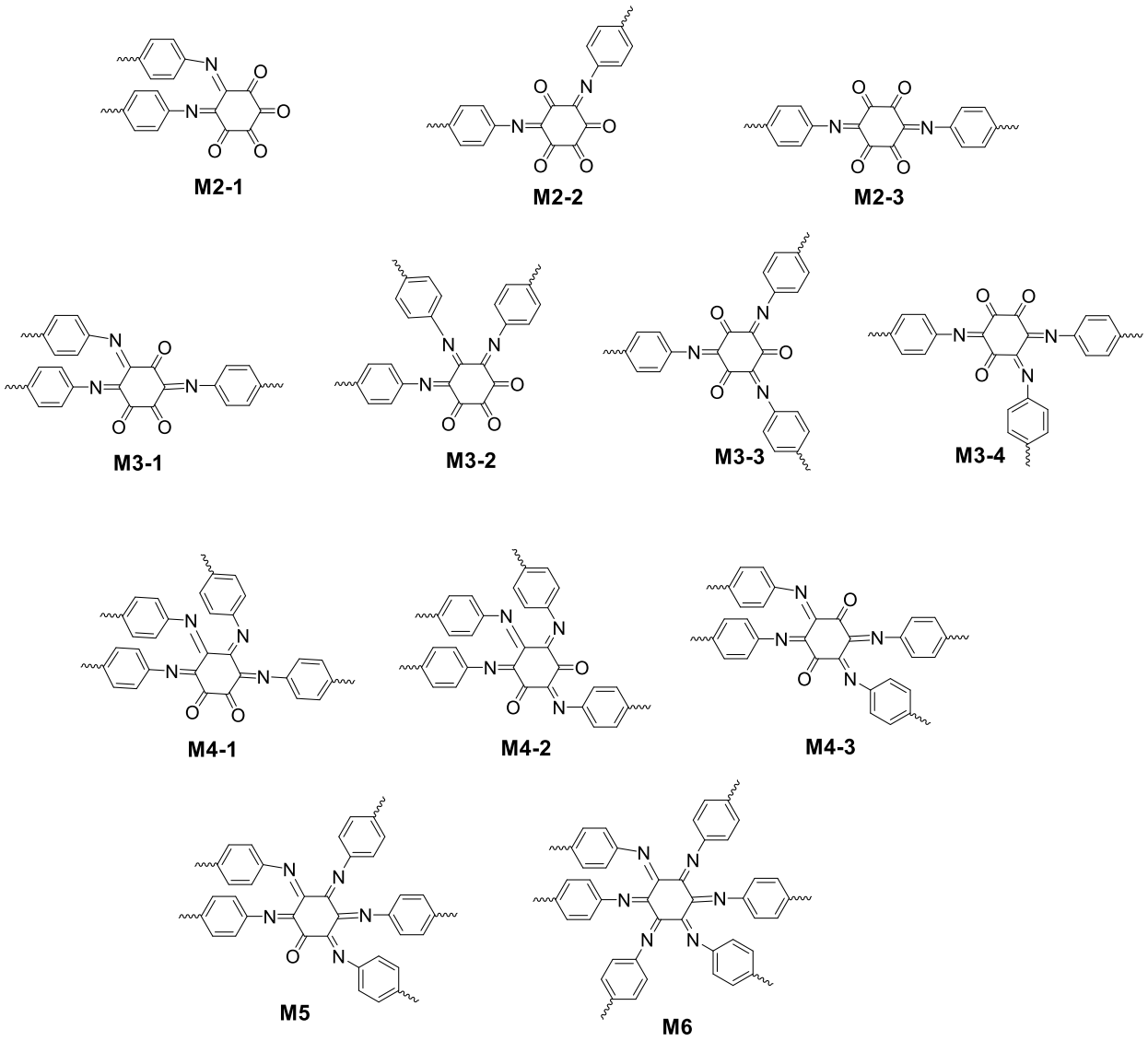

Fig. S1. Structures of the molecular frameworks, which could be formed in the reaction of triquinoyl with 1-2 equivalents of p-phenylenediamine and, thus, represent the building blocks of polymers **P4-P5**

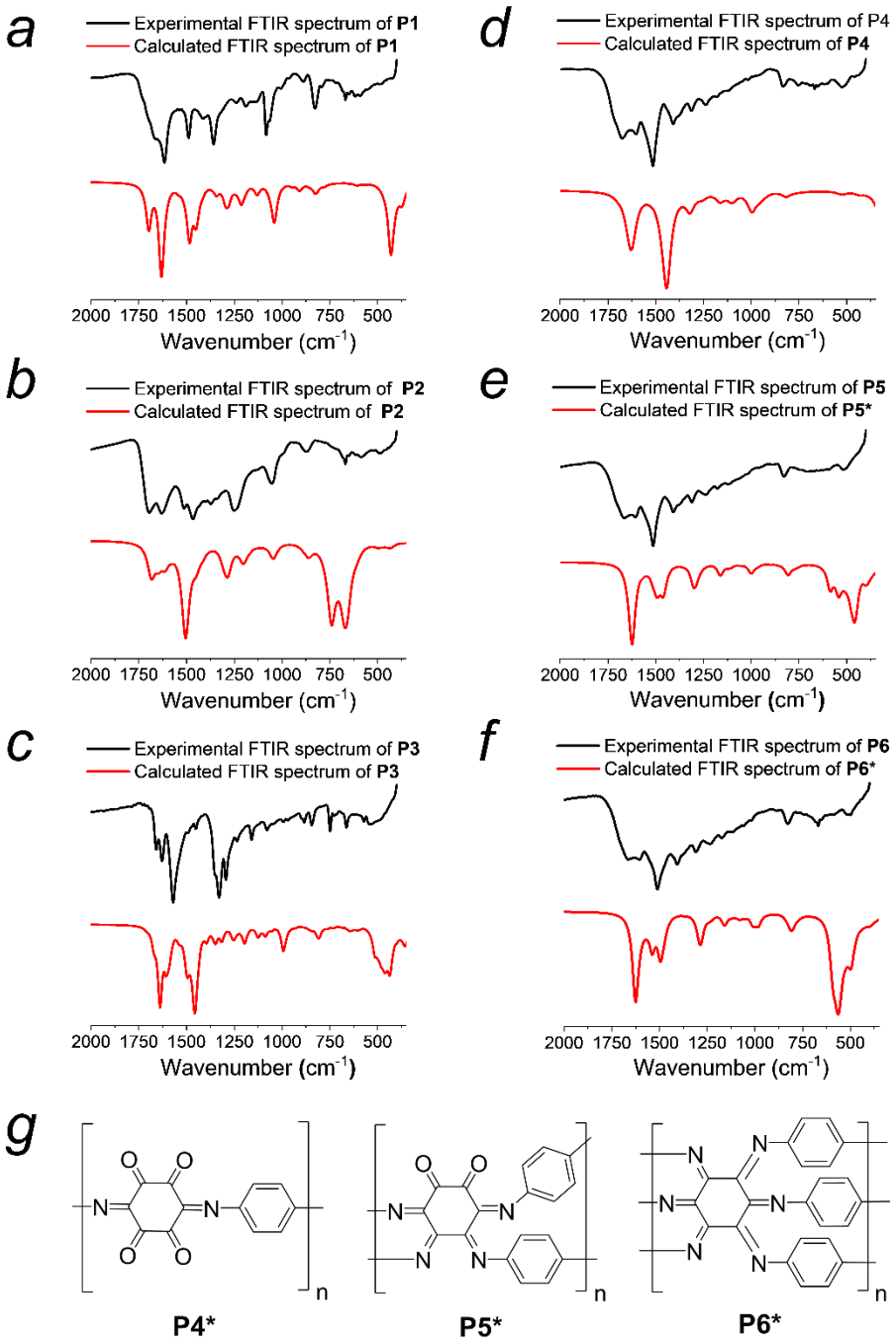

Fig. S2 The experimental and computed FTIR spectra of solid powder of **P1** (a), **P2** (b), **P3** (c), **P4** (d), **P5** (e) and **P6** (f). The model molecular structures of **P4***, **P5*** and **P6*** used for calculations (g) selected due to the reasons explained in the main text.

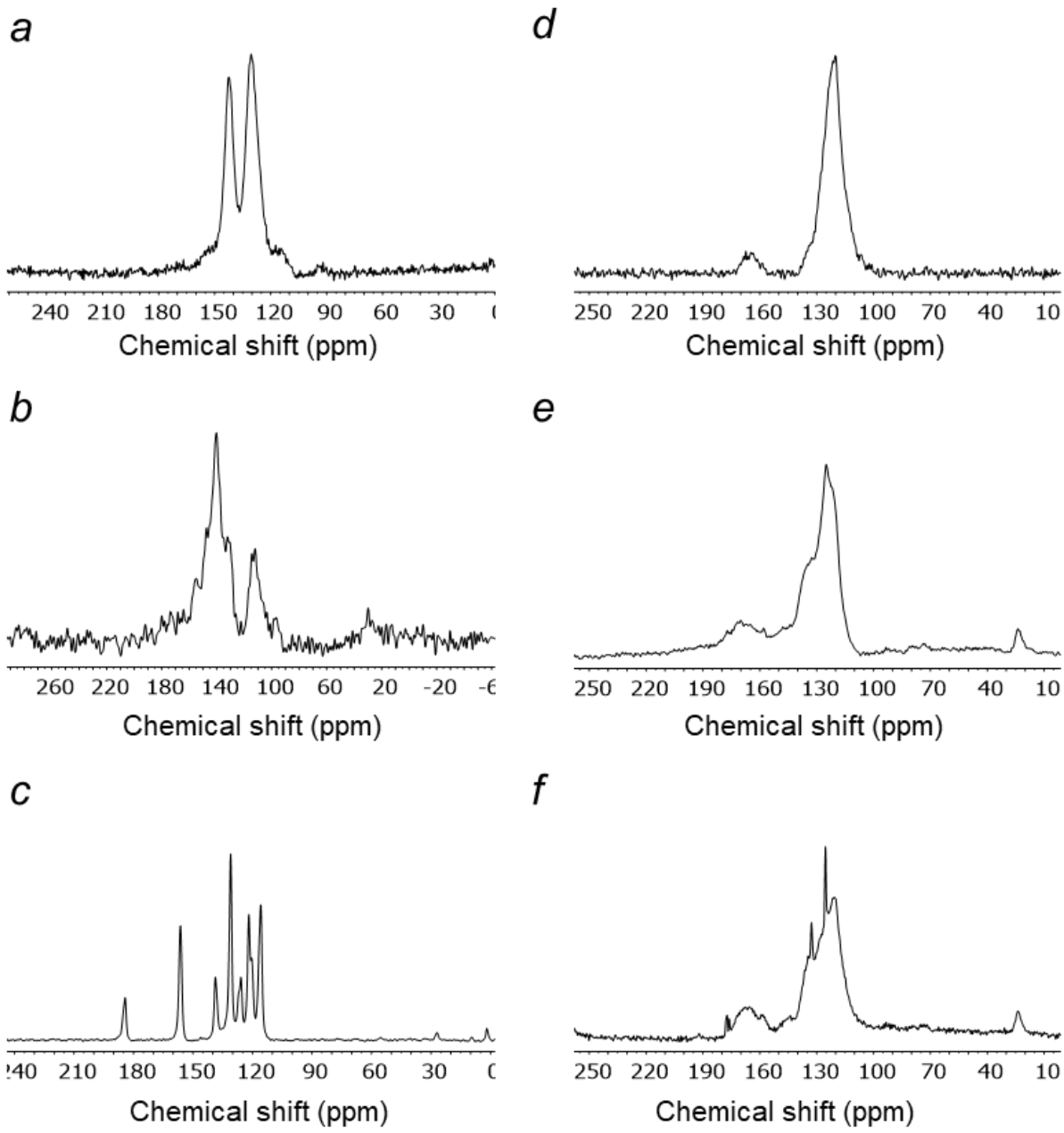

Fig. S3 Solid-state ^{13}C NMR characterization of **P1** (a), **P2** (b), **P3** (c), **P4** (d), **P5** (e) and **P6** (f).

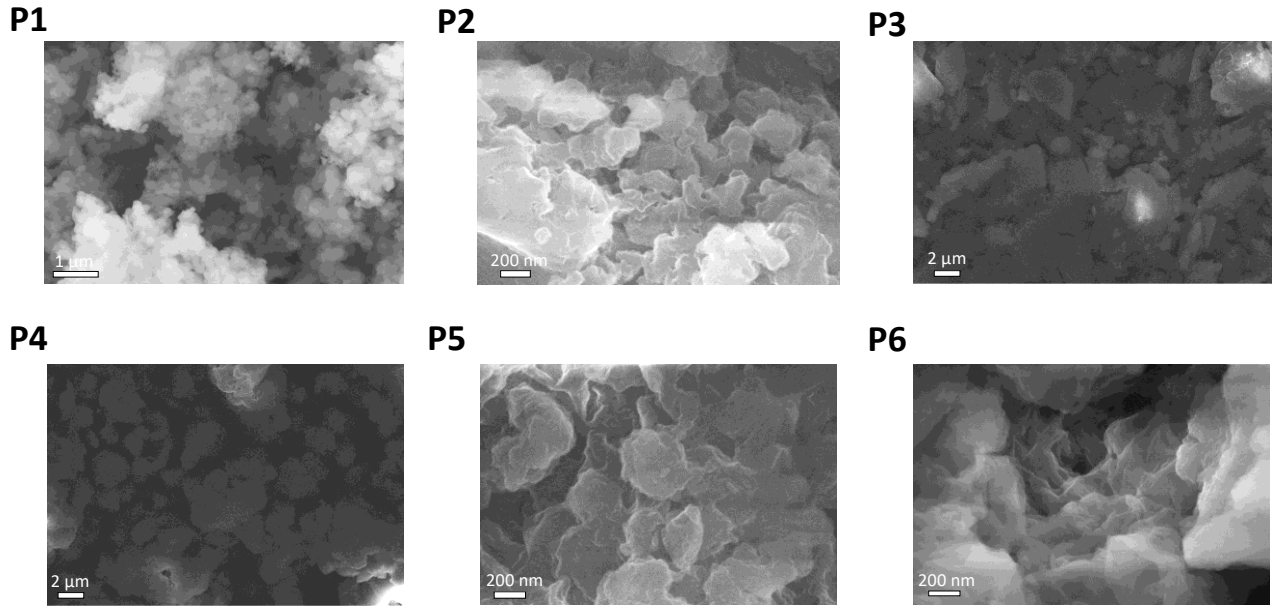

Fig. S4. SEM images of the pristine powders of **P1-P6**

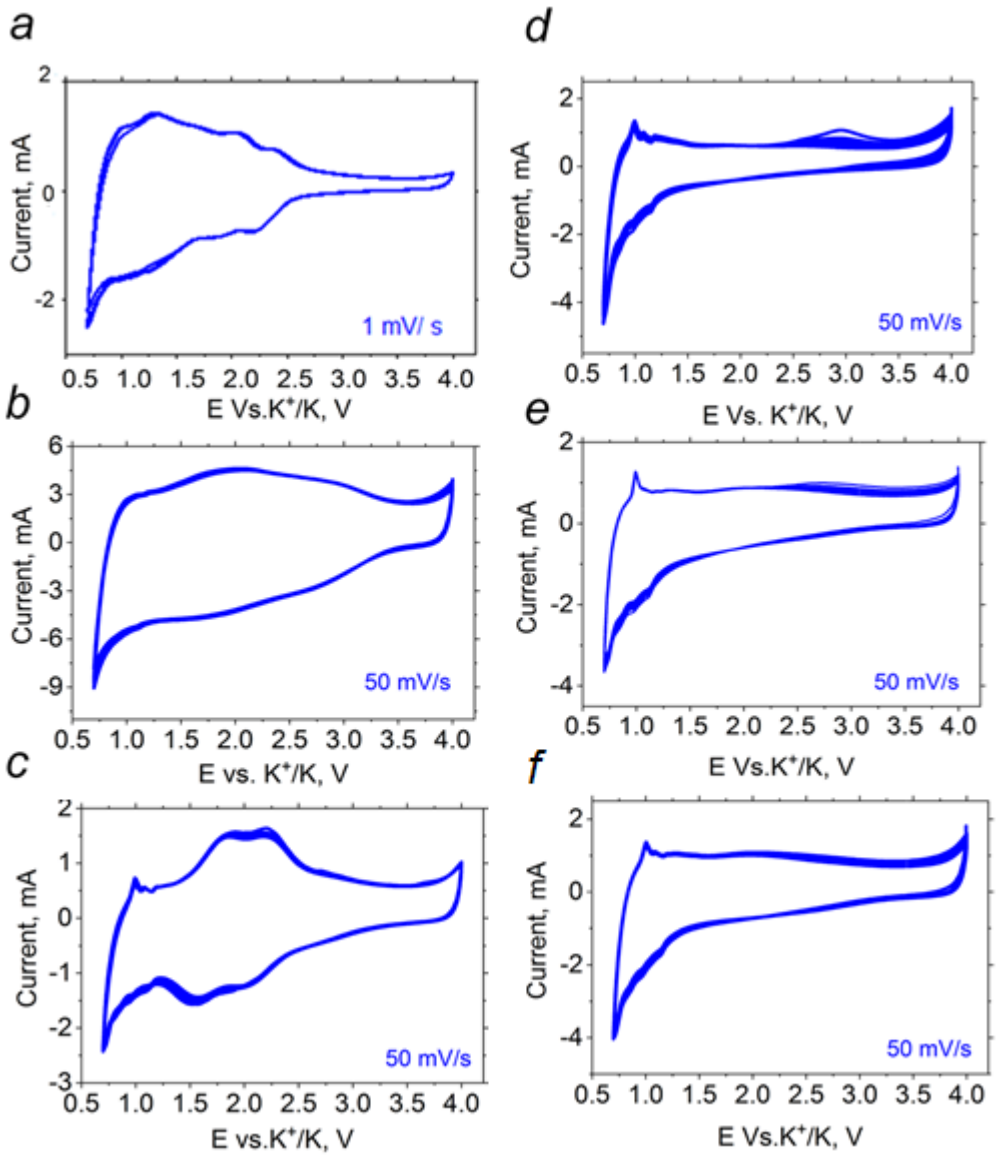

Fig. S5 Cyclic voltammograms of **P1** (a), **P2** (b), **P3** (c), **P4** (d), **P5** (e) and **P6** (f) in half-cells with potassium anodes after galvanostatic pre-conditioning at 0.5 A g^{-1} for a number of cycles required to reach stable capacity after initial activation period.

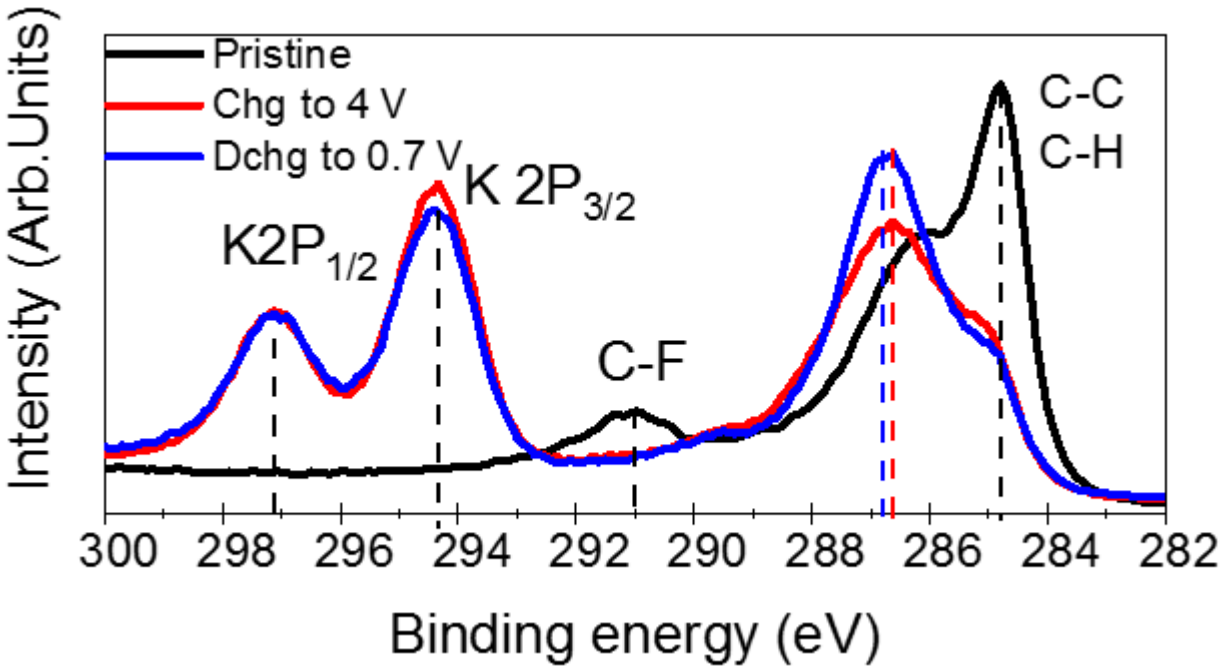

Fig S6. High-resolution core-level C 1s and K 2P XPS spectra of **P1**-based electrode in a pristine state, after first charge to 4 V and after discharge to 0.7 V vs. K^+/K.

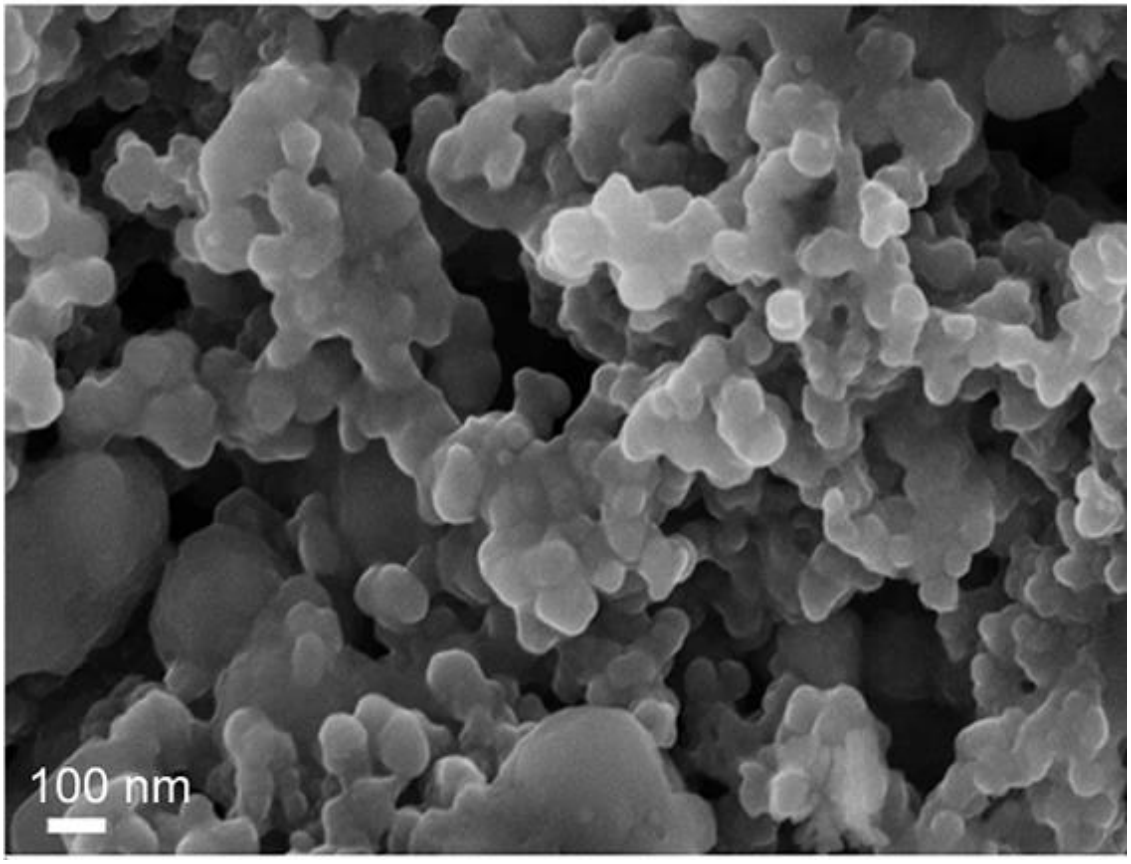

Fig. S7. SEM image of the composite electrode comprised of polymer **P1** after 400 charge-discharge cycles at 0.5 A g^{-1} using 2.2 M KPF_6 in diglyme as electrolyte

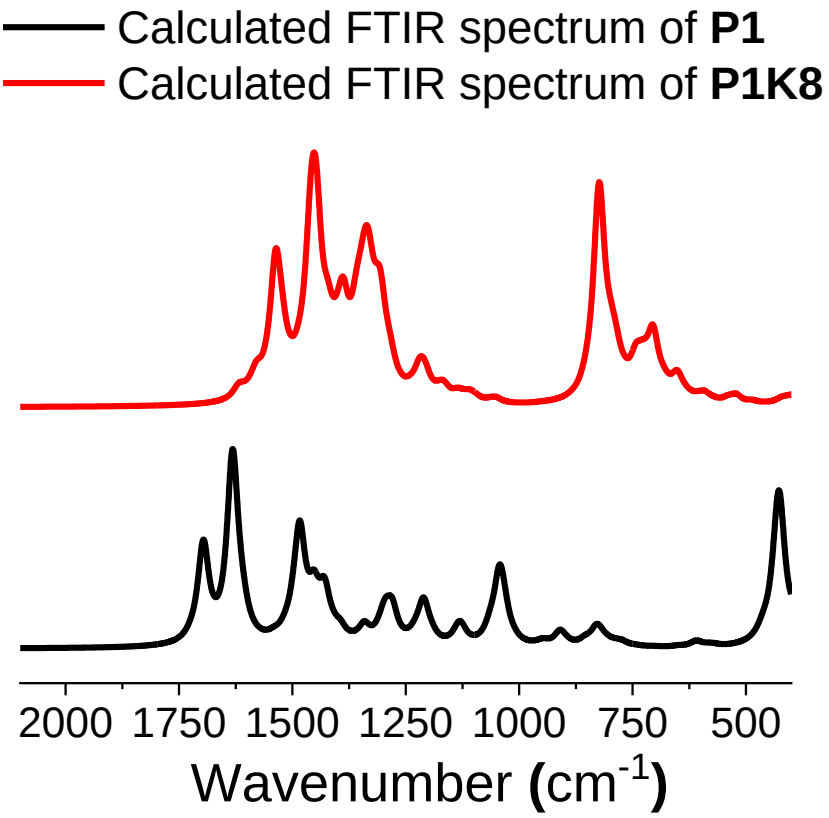

Fig. S8. The comparison of the DFT calculated FTIR spectra of **P1** and its fully metallated form **P18K**.

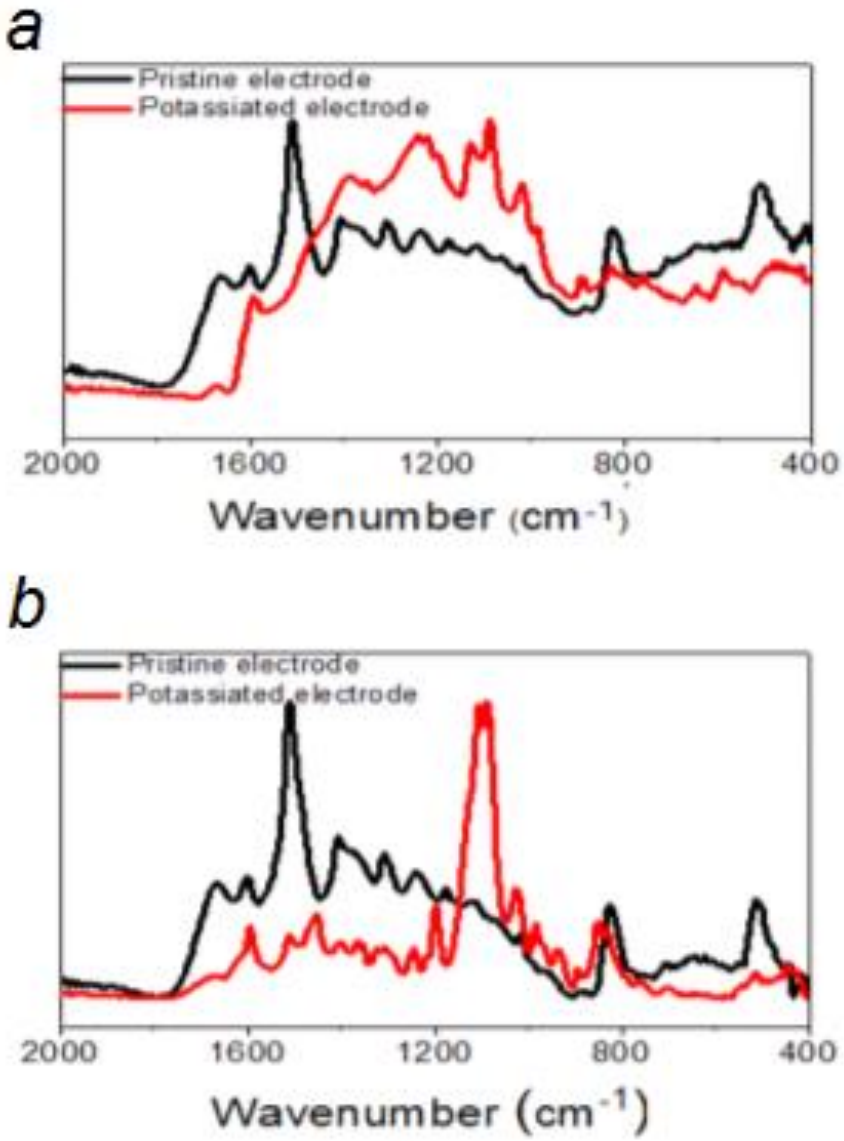

Fig. S9 ATR FTIR spectra of pristine and potassiated electrodes comprised of polymers **P2** (a) and **P4** (b).

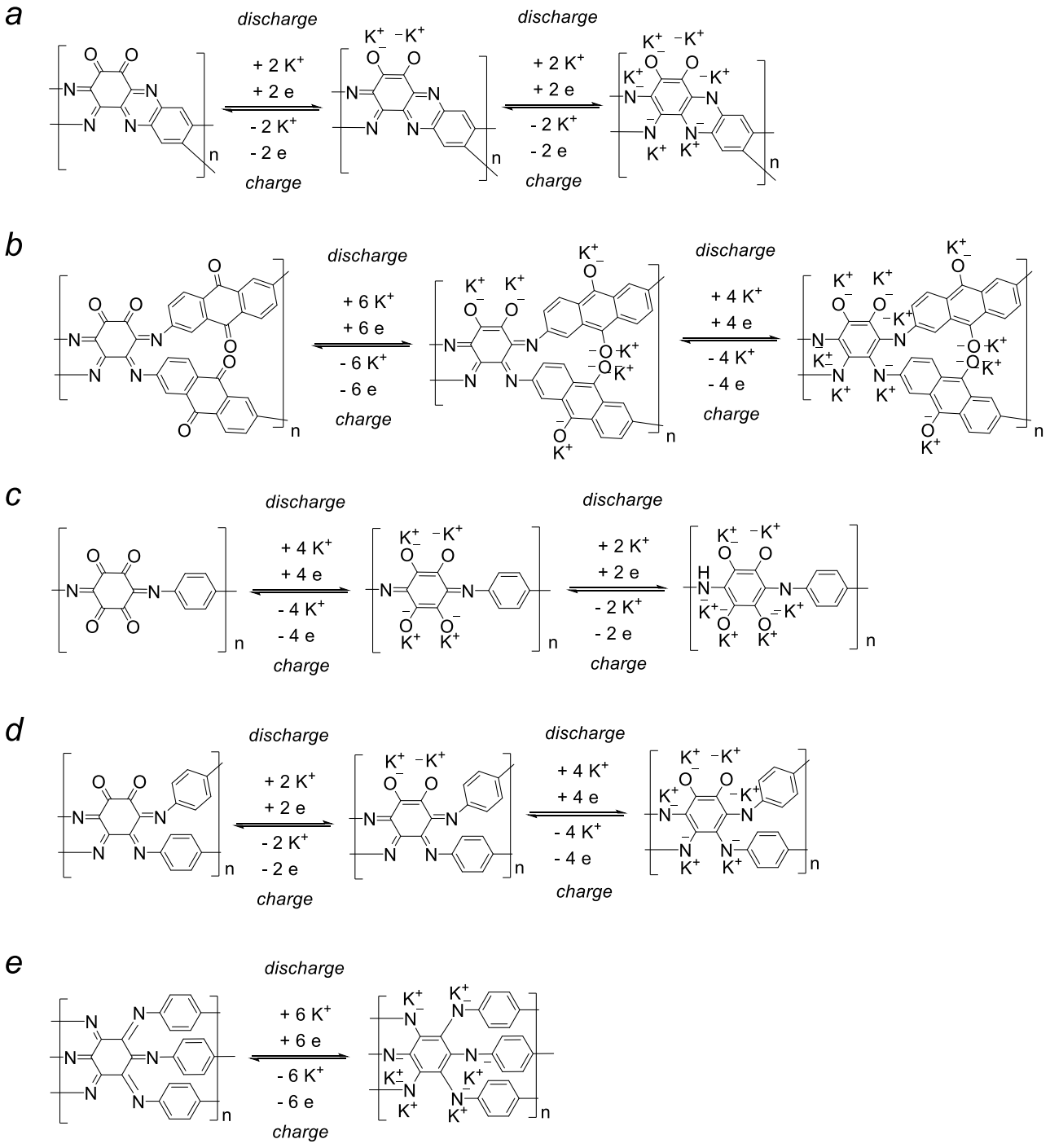

Fig. S10. Redox transformations of **P2** (a), **P3** (b), **P4*** (c), **P5*** (d) and **P6*** (e) upon charging and discharging of potassium half-cells. The model molecular structures **P4***, **P5*** and **P6*** were selected due to the reasons explained in the main text.

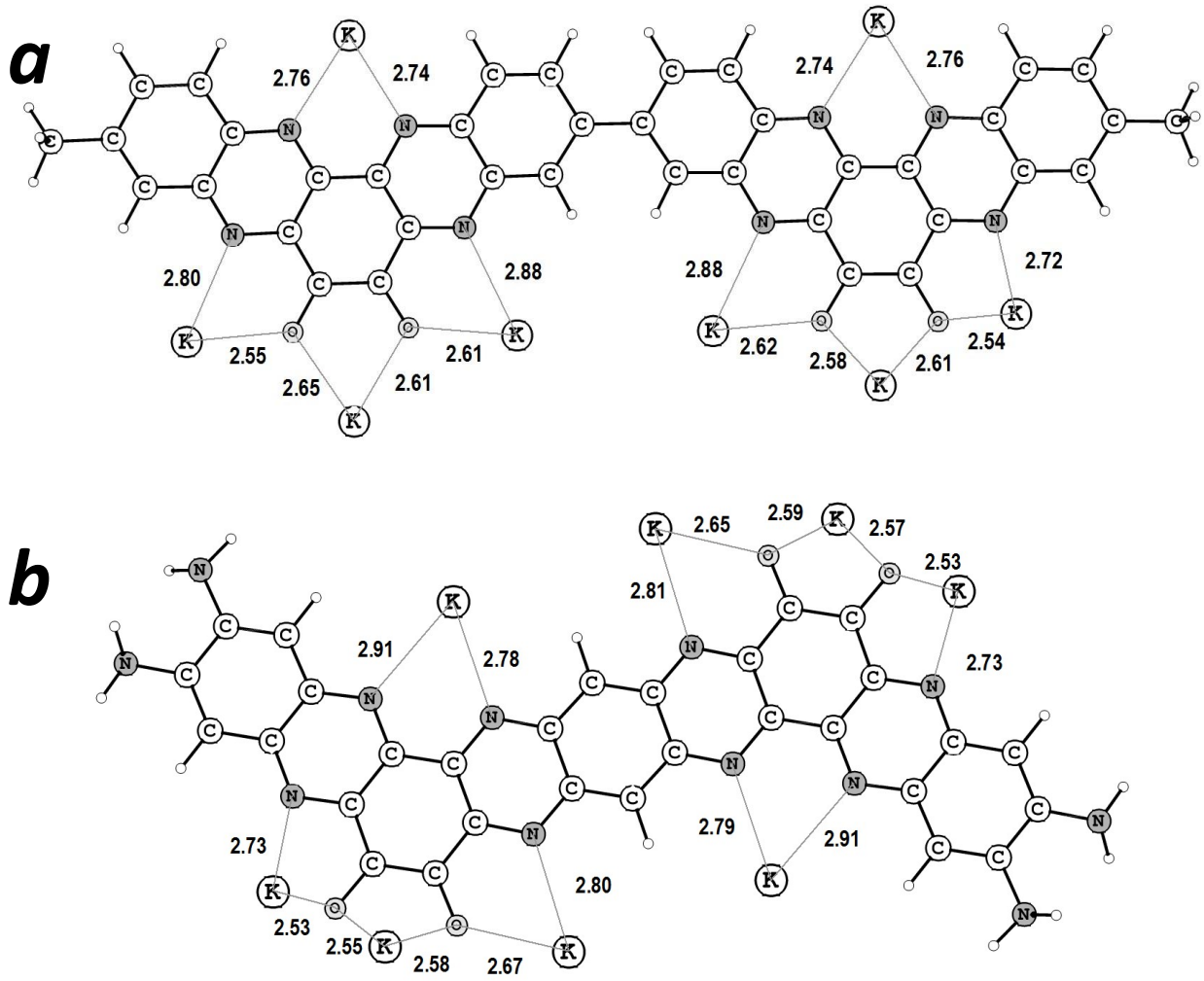

Fig. S11. Computed molecular structures of the oligomeric frameworks resembling polymers **P1** (a) and **P2** (b) after the introduction of 4 K^+ ions and the same number of electrons per repeating unit.

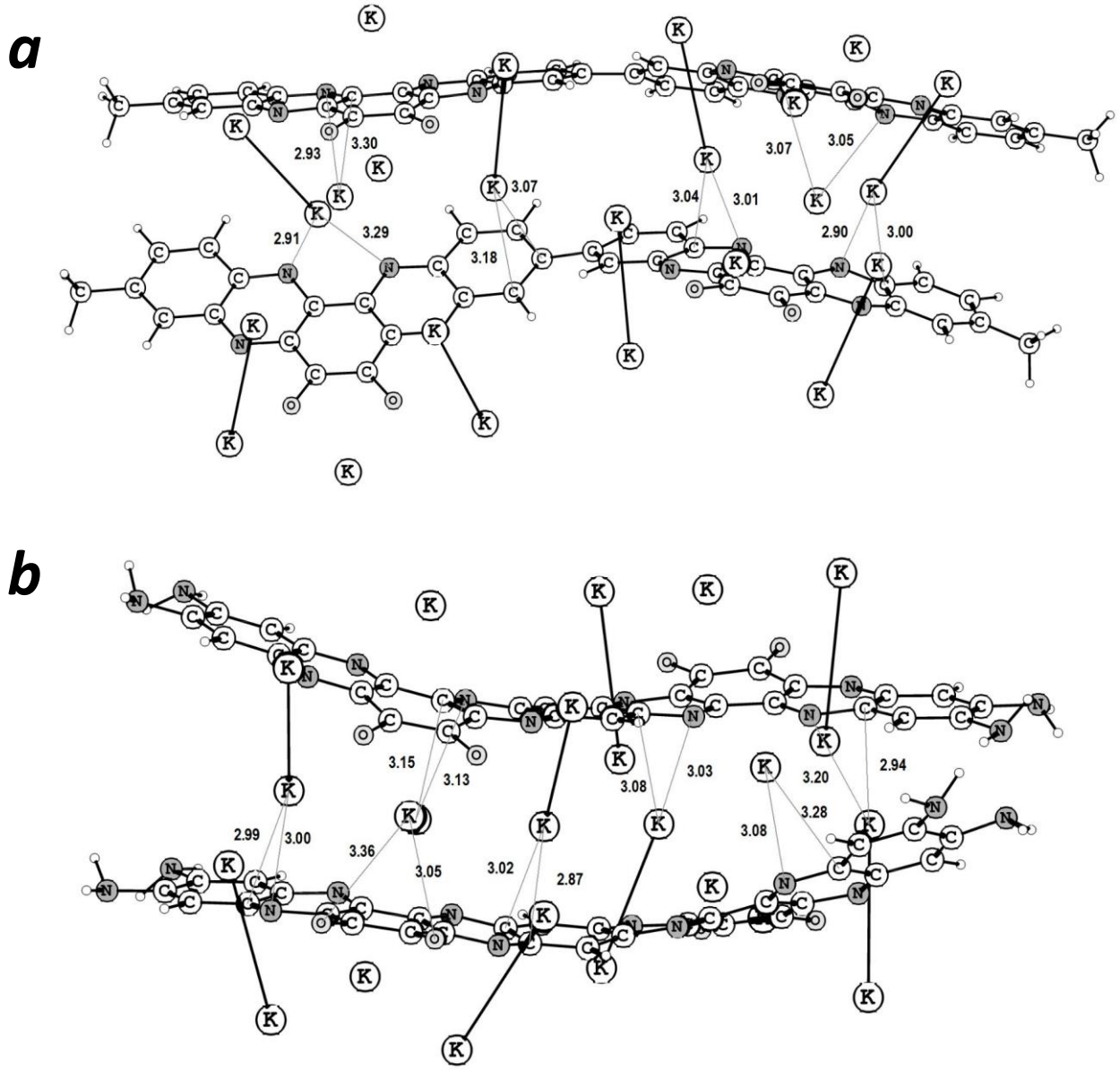

Fig. S12. Computed structures of the supramolecular dimers formed by **P1** (a) and **P2** (b) after the introduction of 6 K^+ ions and the same number of electrons per repeating unit.

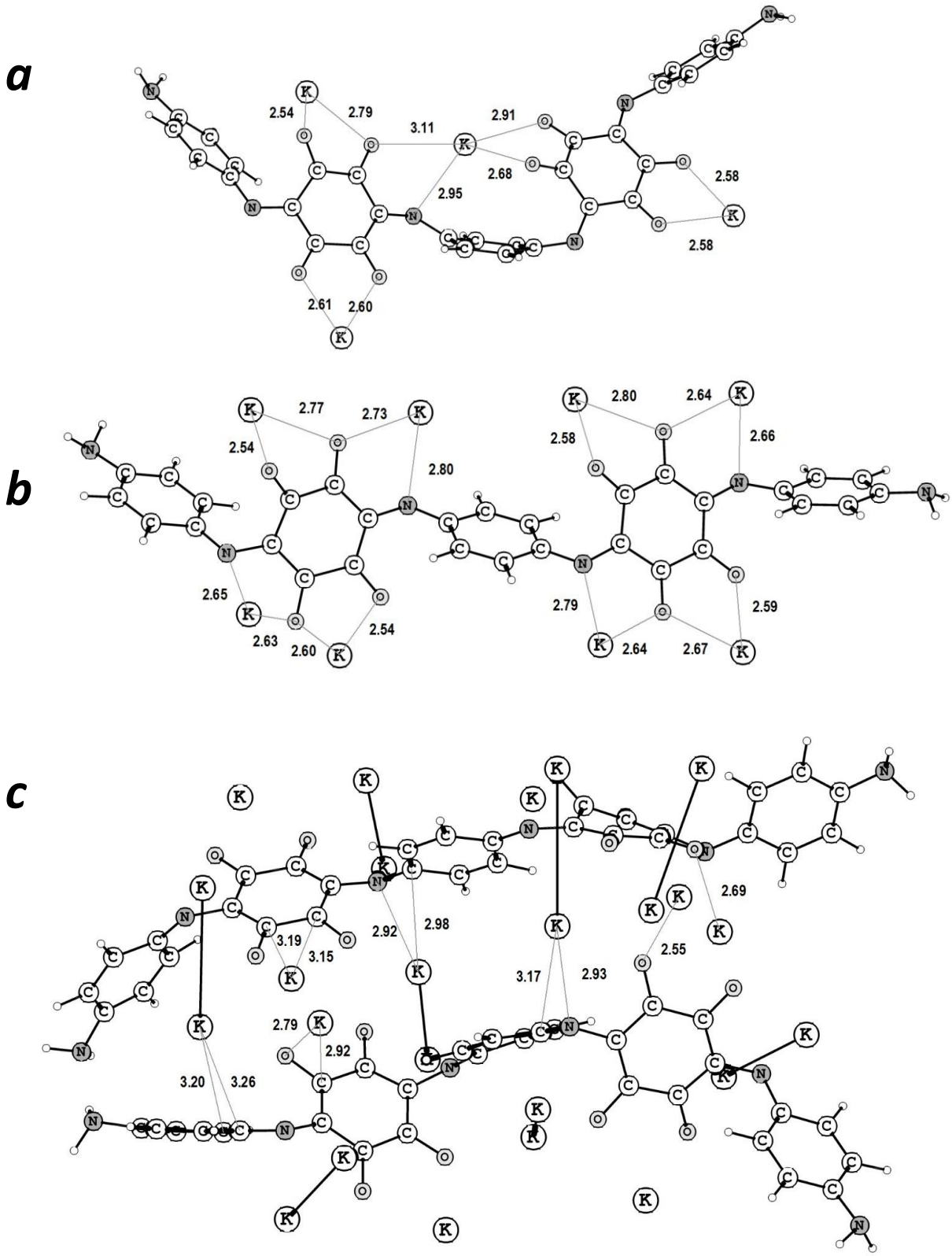

Fig. S13. Computed molecular structures of the oligomeric frameworks of the model polymer **P4*** (see Fig. S2g above) after the introduction of 2 (a), 4 (b) and 6 (c) K^+ ions and the same number of electrons per each repeating unit. The supramolecular dimer structure is shown in (c).

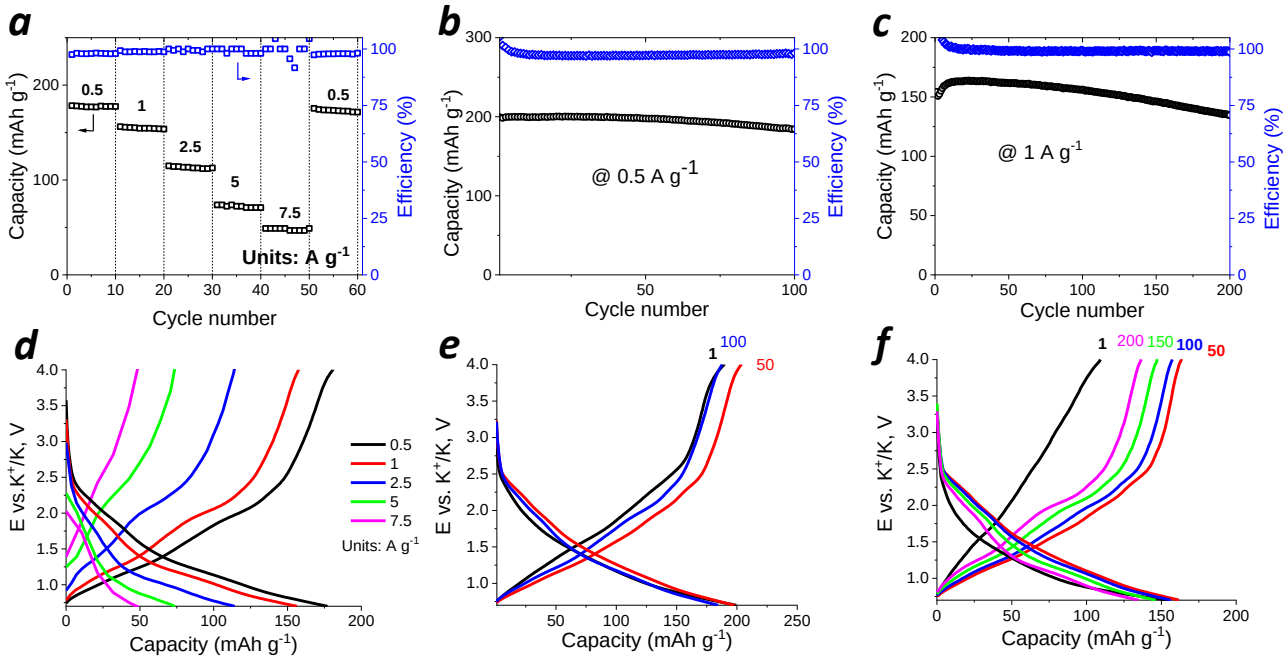

Fig. S14. The rate capability of the electrodes comprised of polymer **P1** with increased loading of 0.7 mg cm^{-2} (a) and the cell cycling behaviour at the current densities of 0.5 A g^{-1}(b) and 1.0 A g^{-1}(c). The corresponding charge-discharge curves are presented in (d-f).

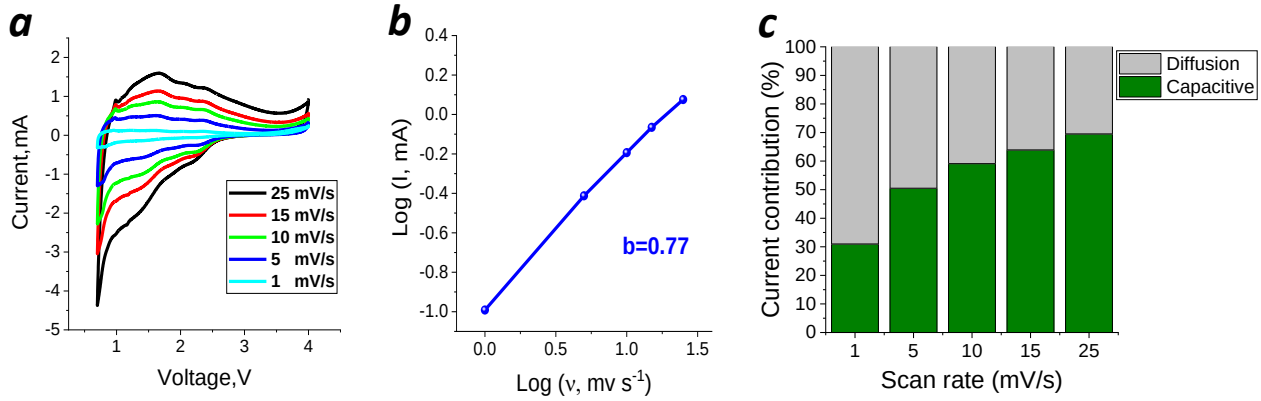

Fig. S15. The CV plots of **P1**//K half-cells recorded at different voltage scan rates (a), the plot of the peak current versus the voltage scan rate (b) and the relative contributions of the capacitive and diffusion currents at different scan rates (c).

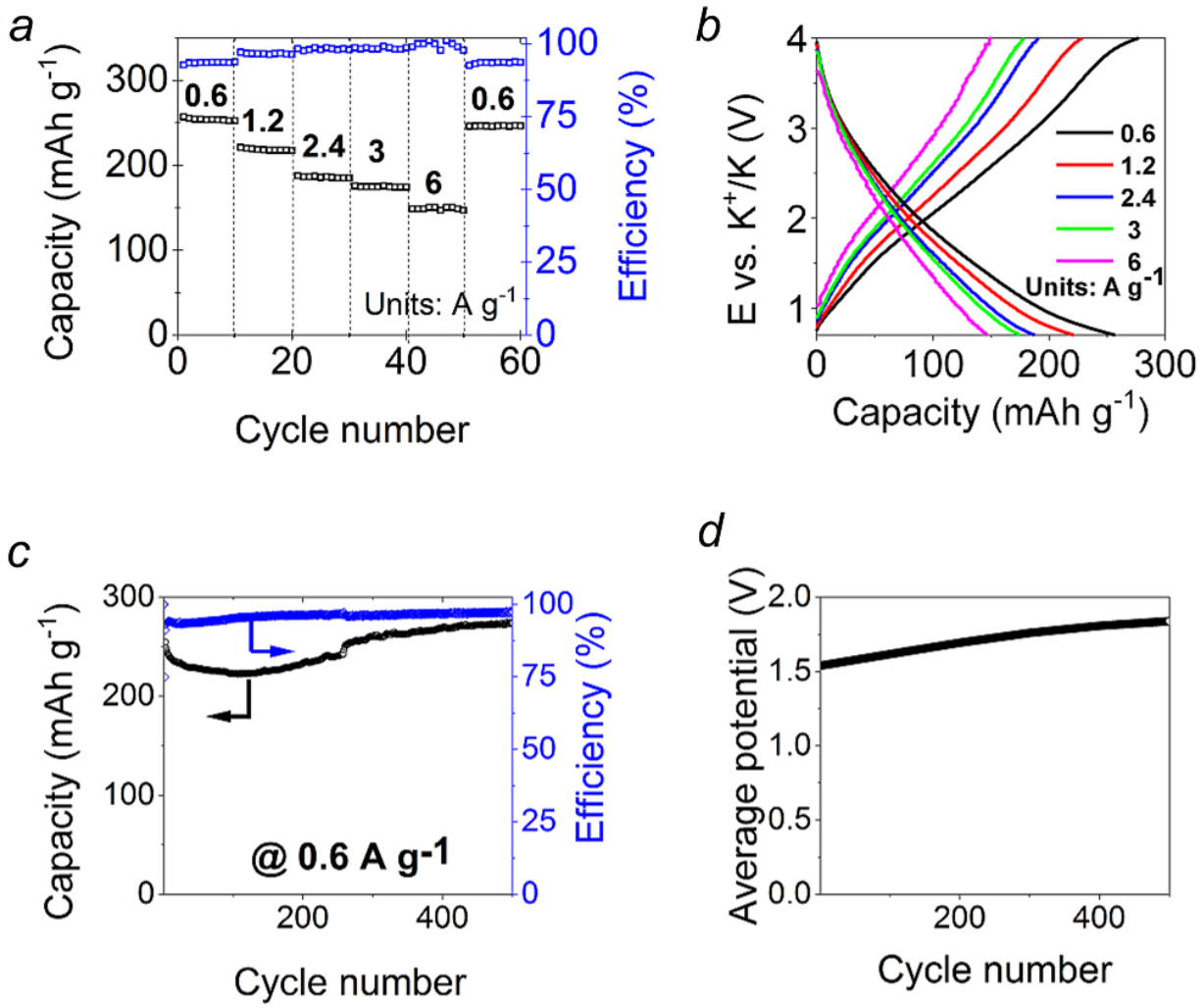

Fig. S16. The rate capability of the electrodes comprised of polymer **P2** (a); charge-discharge curves recorded at different current densities (b); cycling performance of **P2**//K half cells after preconditioning at 0.6 A g^{-1}(c); evolution of the average discharge potential of the cells upon cycling (d).

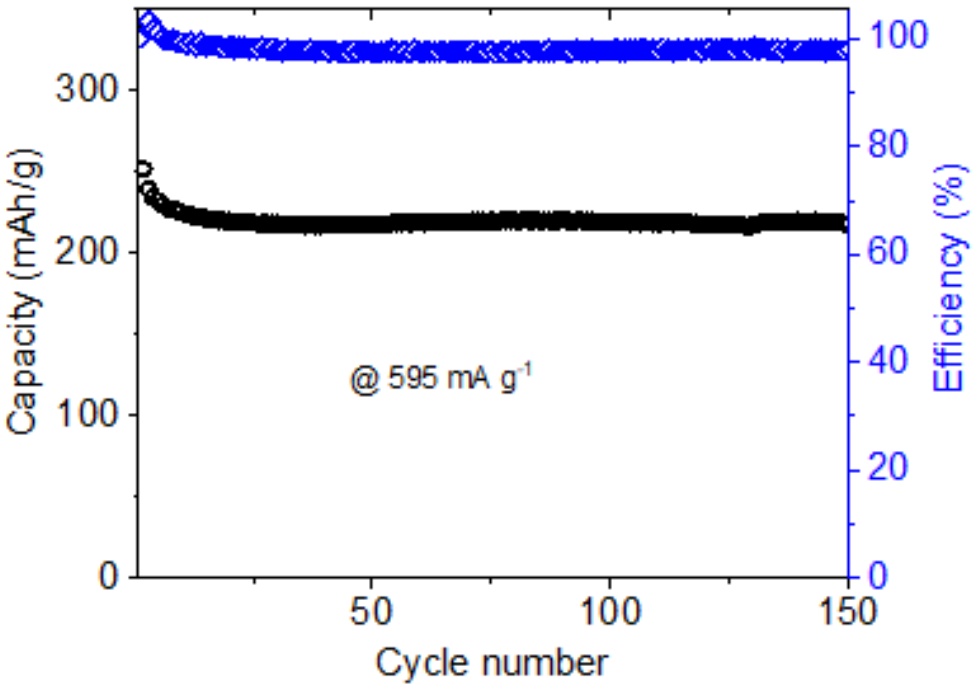

Fig. S17 The cycling behaviour of the cells comprised polymer **P2** with increased areal loading (0.7 mg cm^{-2}) at the current density of 0.595 A g^{-1}

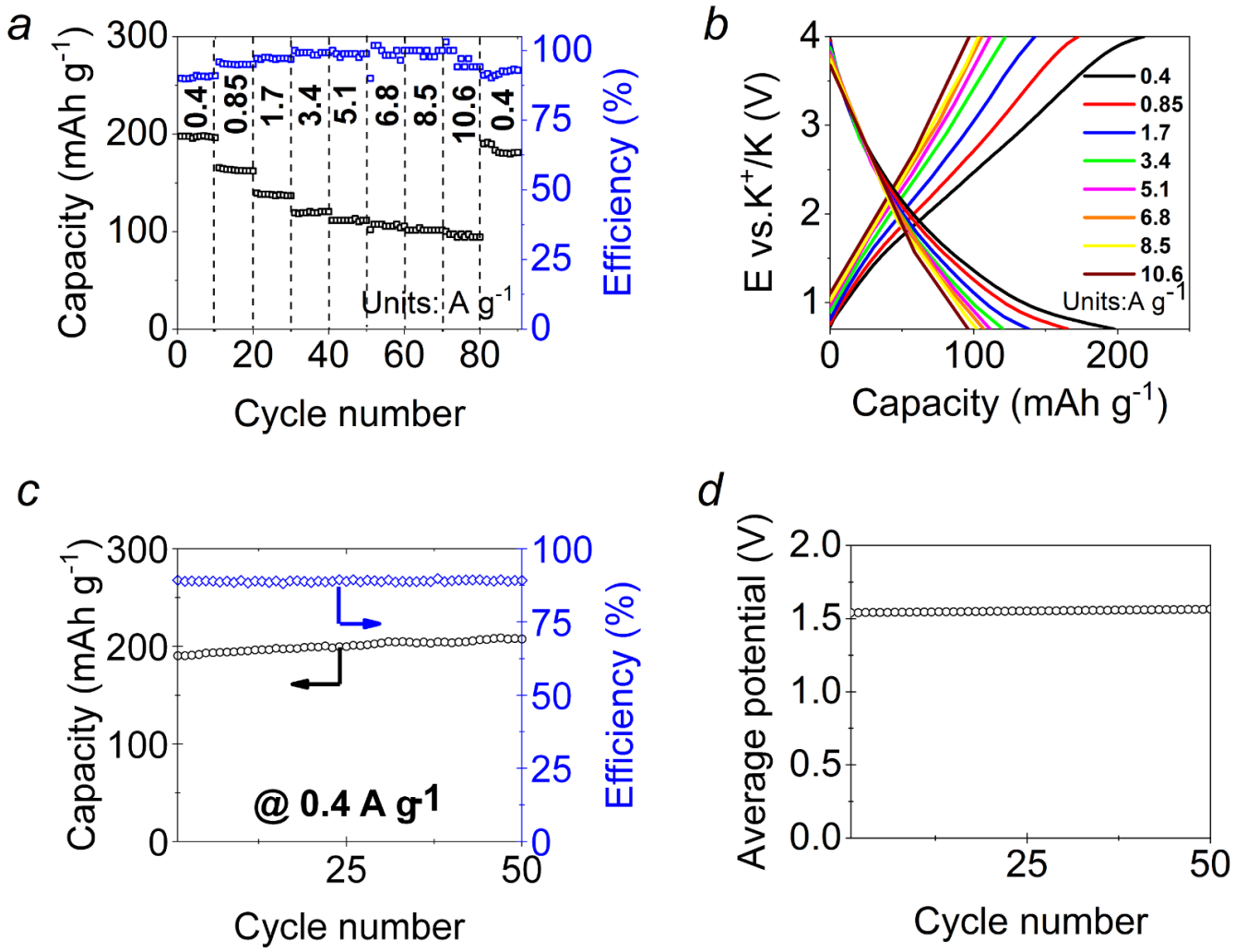

Fig. S18. The rate capability of the electrodes comprised of polymer **P3** (a); charge-discharge curves recorded at different current densities (b); cycling performance of **P3**//K half cells after preconditioning at 0.4 A g^{-1}(c); evolution of the average discharge potential of the cells upon cycling (d).

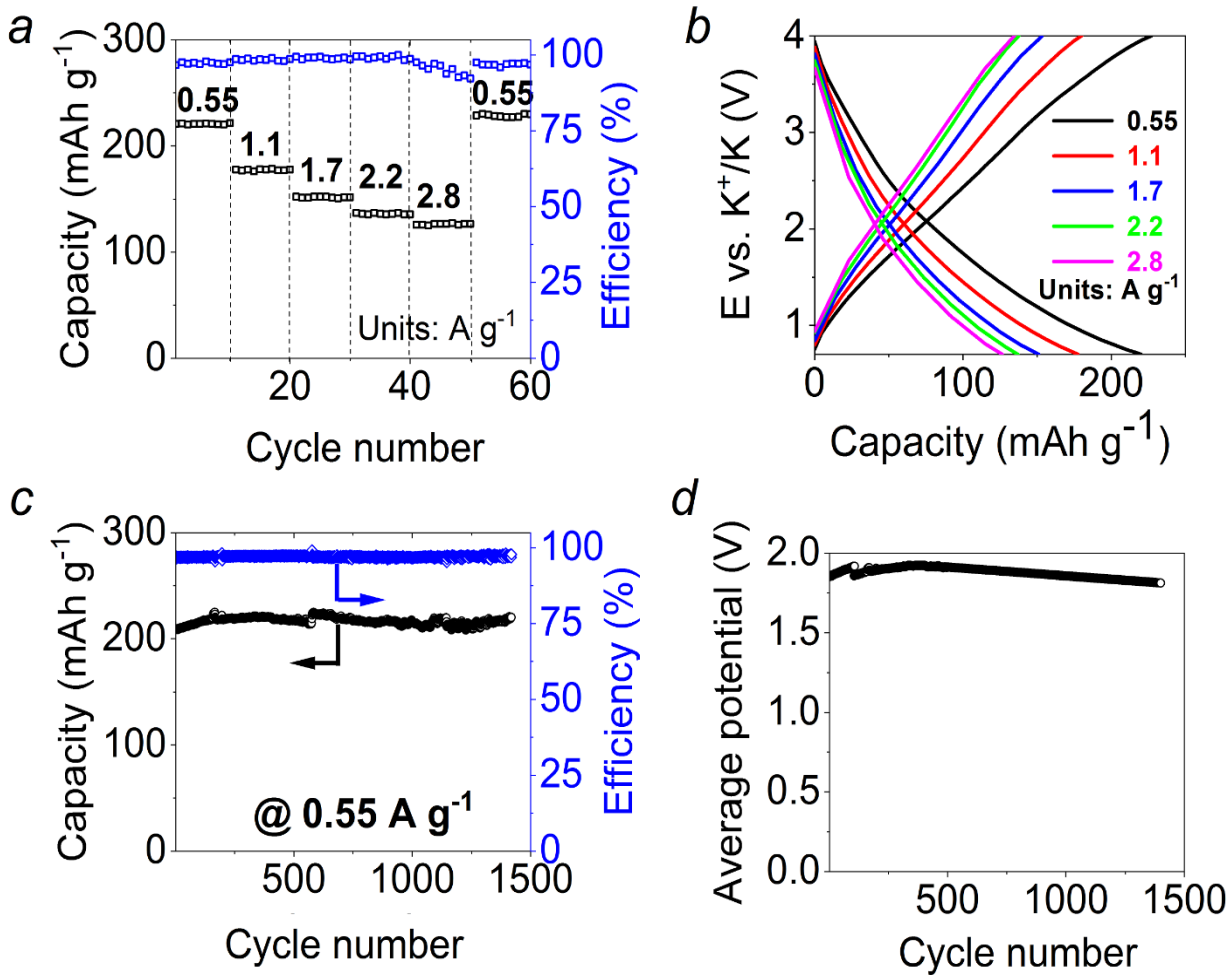

Fig. S19. The rate capability of the electrodes comprised of polymer **P4** (a); charge-discharge curves recorded at different current densities (b); cycling performance of **P4**//K half cells after preconditioning at 0.55 A g^{-1}(c); evolution of the average discharge potential of the cells upon cycling (d).

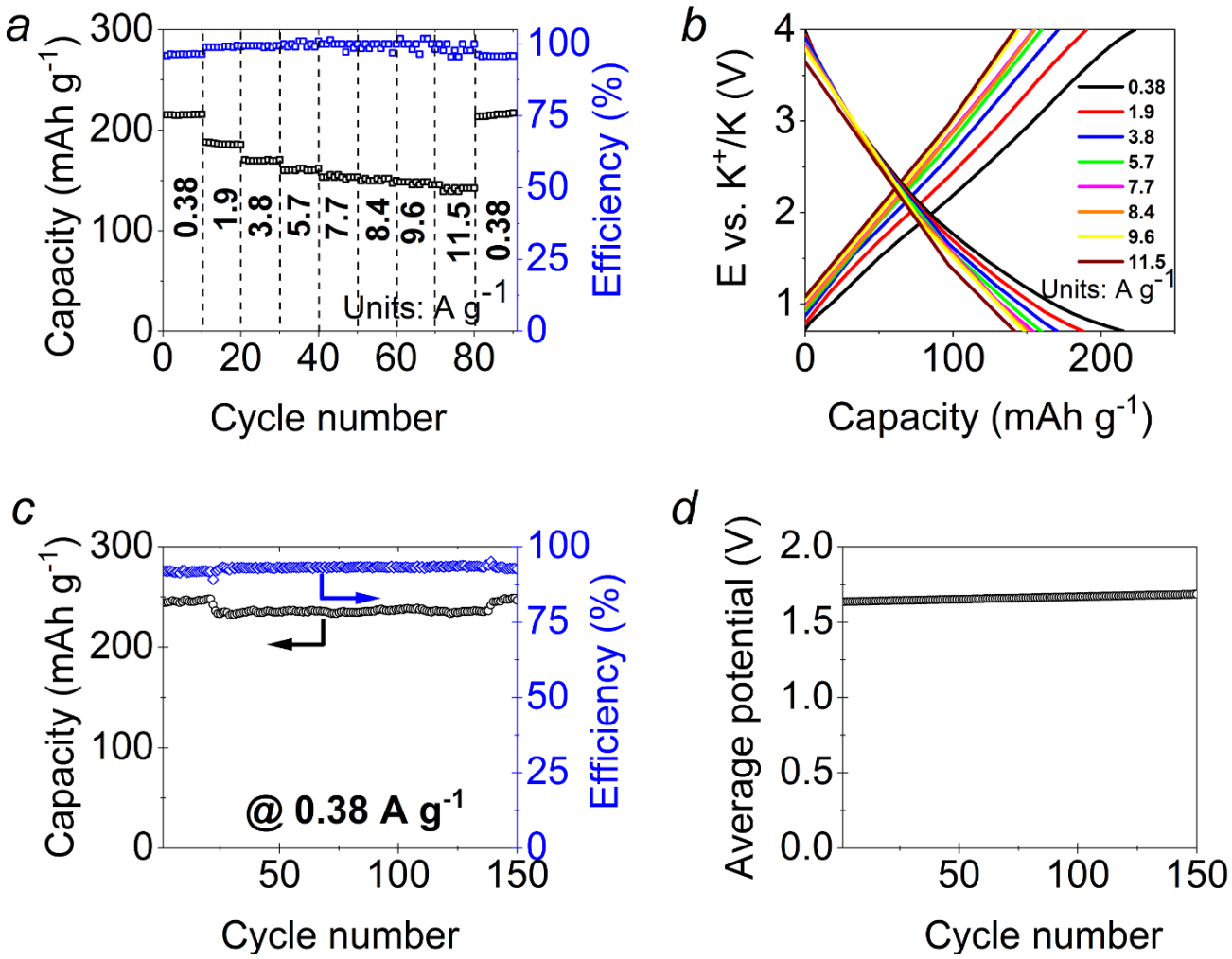

Fig. S20. The rate capability of the electrodes comprised of polymer **P5** (a); charge-discharge curves recorded at different current densities (b); cycling performance of **P5**//K half cells after preconditioning at 0.38 A g^{-1}(c); evolution of the average discharge potential of the cells upon cycling (d).

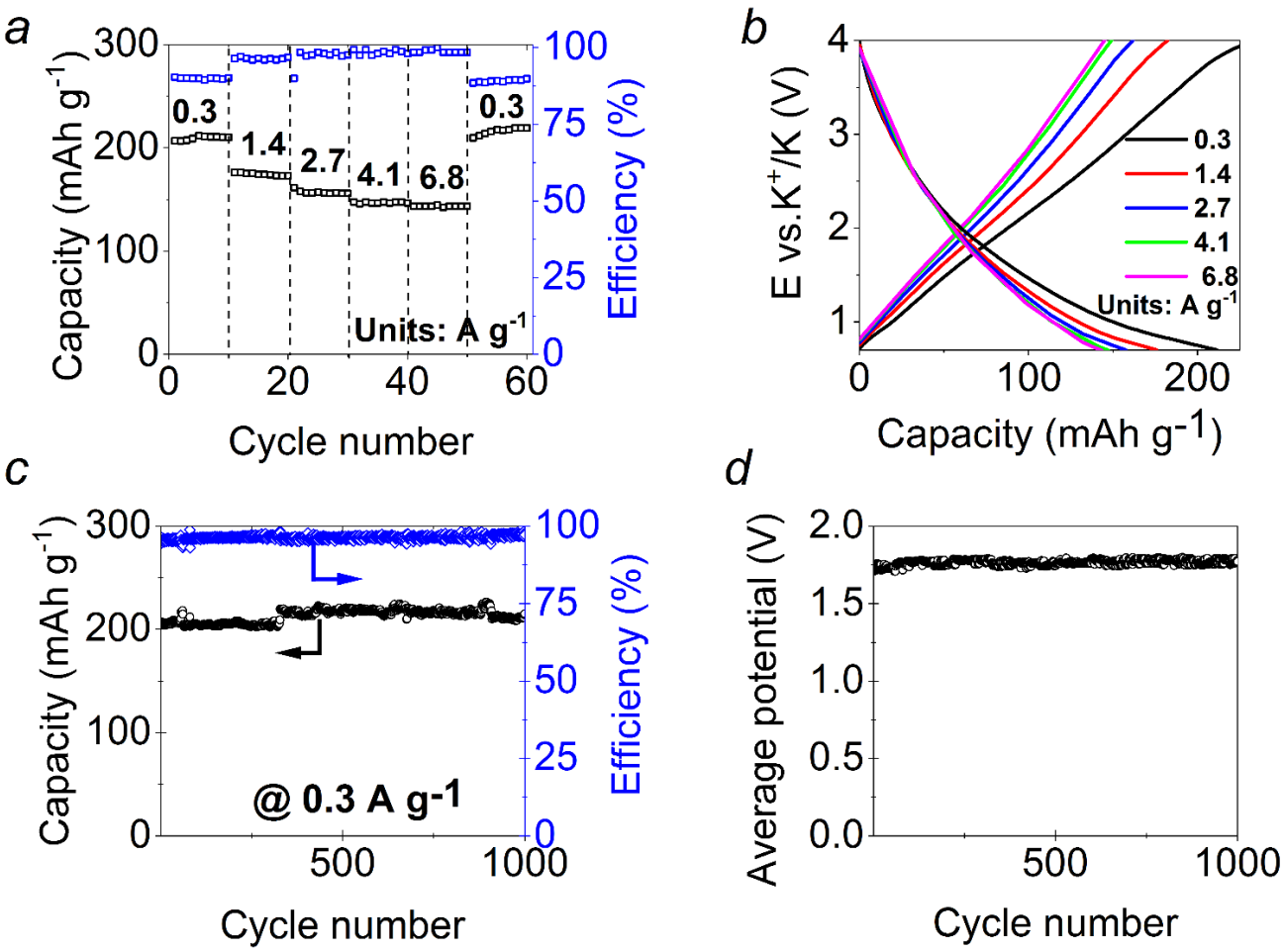

Fig. S21. The rate capability of the electrodes comprised of polymer **P6** (a); charge-discharge curves recorded at different current densities (b); cycling performance of **P6**//K half cells after preconditioning at 0.3 A g^{-1}(c); evolution of the average discharge potential of the cells upon cycling (d).